Impacts of Tertiary Ligands in Catalysis in Thermostable Human Carbonic Anhydrase II by Site-directed Mutagenesis and Genetic Code Expansion*

Danielle M. Stevens[1], Mai N. Le, Youngmin Park, and Jacob W. Mazzola
Department of Biochemistry and Biophysics, Oregon State University, Corvallis, Oregon 97330, United States

ABSTRACT: Carbonic anhydrases are ubiquitous enzymes that catalyze the reverse hydration and dehydration of carbon dioxide and bicarbonate respectively. A variety of tumors in humans show overexpression of human carbonic anhydrase II (HCA II) leading to an acidic breakdown of carbon dioxide into bicarbonate. While a variety of drug inhibitors exist, many come with undesirable side effects. Using non-conical amino acids (ncAAs), we probe an adjacent residue (Phe 93) to one of three key histidine residues involved in the active site. This shifting of a histidine residue creates a non-optimal proton transfer and thus, decreasing catalytic efficiency. The goal of this study was to better understand the catalytic flexibility and efficiency of HCA II without compromising protein stability. What we found was unexpected: exchanging phenylalanine with *p*-bromophenylalanine (pBrF) has a slight decrease in enzymatic activity while the exchange with *p*-nitrophenylalanine (pNO_2F) significantly increased enzymatic activity in both an optimal pH of 7.4 and a more acidic pH of 6.4 compared to WT HCA II. In addition, stability of pNO_2F mutant protein is significantly increased in pH conditions ranging from 7.4 to 9.4 compared to wild-type HCA II. Finally, the stability of pBrF mutant is comparable or even slightly higher than wild-type HCA II in pH conditions ranging from 7.4 to 9.4. This data suggests that Phe 93 plays a role in influencing the coordination of His 94, one of three key residues that coordinate a zinc ion involved in protein transfer; additionally, further studies of this residue may lead to potential cancer treatments based on the pBrF mutant and industrial applications based on the pNO_2F mutant.

Carbonic anhydrase II is considered one of the fastest enzymes in the human body with a catalytic turnover of 1 μs^{-1} for the hydration of CO_2 (*1*,*2*). Expressed in a variety of tissue types, HCA II contributes to a wide range of catabolic processes including the breakdown of CO_2. The metalloproteins carry out the chemical conversion of carbon dioxide and water into bicarbonate through the zinc-bound atom in the active site (reaction 1) (*1*).

(1) $CO_2 + EZnOH^- \leftrightarrow ZnHCO_3^- \leftrightarrow EZnH_2O + HCO_3^-$

The monomeric enzyme with a molecular weight of 29 kDa exists and predominantly functions in the cytosol (*3*). An analysis of its tertiary structure reveals a 15 Å deep binding pocket lined with hydrophobic residues. Its active site includes His 64 (not shown) and one zinc ion in tetrahedral geometry with three histidine residues (His 94, 96, 113) with bound water/hydroxyl ion (Figure 1A) (*2*,*4*). Based on defined crystalline studies, the active site of HCA II shows that CO_2 is positioned 2.8 Å from the zinc-hydroxide allowing for a nucleophilic attack by their lone pair of electrons (*1*).

Crystalline structure of HCA II shows a central region of seven beta sheet strands which help form the hydrophobic pocket containing ligands which are directly and indirectly involved in coordinating the zinc ion metal center (*5*). These structures have also shown that all zinc-ligand distances are about 2.1 Å in length (*6*). Previously, studies have shown that there is a hierarchy of ligands involved with zinc coordination. According to Cox et al., the first shell of residues directly involved in binding to the zinc ion are His 94, His 96 and His 119 (*7*). Secondary ligands such as Gln 92, Glu 177, and Asp 244 pay a role in stabilizing the primary ligands, His 94, His 117, and His 96

* This work was funded though lab fees paid collectively by OSU students enrolled in Biochemistry Laboratory.
[1] First Author.

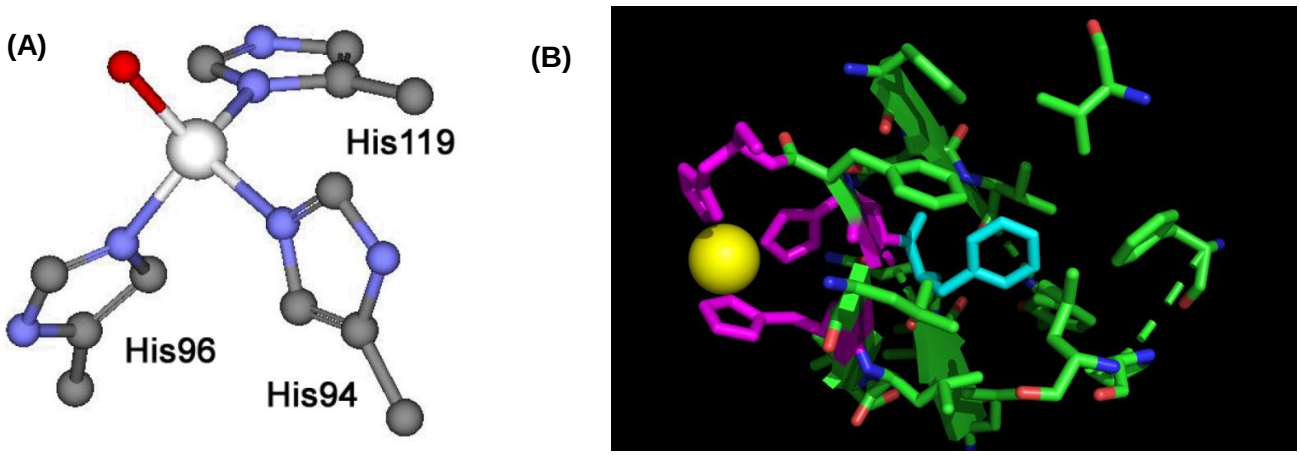

Figure 1: Structure of the HCA II-Zn2+ complex. (A) Zinc coordination in the active site of HCA II (*4*). **(B)** Hydrophobic patch outside of zinc coordination site. Image shows connection between His 93 (pink) and Phe 94 (cyan) on beta sheet. Figure was made using PyMol (DeLano Scientific).

respectively, for optimal zinc ion coordination (*7*). Finally, the third shell ligands such as Phe 93 and Phe 95 play a role in anchoring the beta-strand that contains His 94 and His 96 (*7*). According to Cox et al., Phe 93 is a tertiary ligand that does not directly impact the stabilization of His 94 in position for the necessary zinc ion coordination (*7*). Mutagenesis of residues flanking the primary ligands, Phe 93 and Phe 95, have been shown to not affect catalytic activity (*8*). Otherwise, few studies have studied the role Phe 93 in affecting catalytic activity since. We, therefore, use site-directed mutagenesis to study the flexibility of the active site and the role secondary/tertiary ligands can have on catalytic activity through adjacent residue Phe 93.

In this presented work, Phe 93 will be replaced with *para*-bromophenylalanine (pBrF) and then *para*-nitrophenylalanine (pNO_2F) to probe whether we can shift residues in the active site to reduce enzymatic function without compromising stability through genetic code expansion. Specifically, these two non-conical amino acids were chosen based on their unique chemical properties; both are electron-withdrawing groups and their overall size varies, the atomic space of the bromine atom is greater than the preexisting hydrogen atom and the nitro group being even greater in space. In addition, pNO_2F is a much stronger electron withdrawing group, so it is expected to have a greater pull on adjacent residues compared to pBrF. This will, in turn, result in a larger shift of the histidine residues inward to the zinc atom (Figure 1B). This study will reveal the flexibility of the active site by shifting an adjacent phenylalanine residue (site 93), a part of the beta-strand toward the other enzymatically involved histidine residues (Figure 1B). In doing so, we sought to decrease enzymatic activity without compromising stability in thermostable HCA II (*9*). By utilizing a thermostable variant, we hypothesize that this will limit additional shifting of other residues, maintain tight packing, and preserve its high stability (*9*). By analyzing the changes in enzymatic rate and protein stability, we will determine a more detailed characterization of the active-site through the secondary and tertiary ligands in the hydrophobic pocket of HCA II.

Further characterization of HCA II has key clinical applications. Previous clinical studies have found that a variety malignant tumors contain high expression of carbonic anhydrase II and may be implicated in tumor metabolism (*10*). Specifically, they have shown that high expression in the endothelium leads to brain, lung, renal, and esophageal cancers (*10*,*11*). Tumor environments are more acidic, which may be mediated by HCA II (*10*). Specifically, acidic microenvironments can aid in the regulation of this cellular phenotype (*12*). There have been numerous inhibitors studied for treatment of these cancers but many come with numerous side-effects (*4*). We hypothesize that by probing nearby residues involved in the active site with non-canonical amino acids of differing size, we can decrease the enzymatic activity (kcat) without compromising either substrate binding (km) or stability (T_M). This information will help us gain insights into the flexibility of the active site and

the overall stability of the protein. Increased knowledge of active site and its functionality can potentially aid in the development of an antagonist to carbonic anhydrase II for directed cancer therapy.

MATERIALS AND METHODS

Expression and purification of wild-type enzyme. All bacterial cultures were incubated in a 37°C shaker for 48 hours. E. coli DH10**β** carbonic anhydrase II (CA) and ncAA mutants starter cultures were grown in non-inducing media. Expression of carbonic anhydrase II was introduced by pBAD-CA and tRNA-synthetase necessary for ncAA integration was introduced by pDULE-pCNF into competent DH10**β** cells. Expression and selection for pBAD-CA and pDULE-pCNF was initiated through the addition of 750 µl of starter culture into 75 mL of autoinduction media containing ampicillin (100 µg/mL) and tetracycline (25 µg/mL) and respective ncAA (*13,14,15*). ncAA pBrF and pNO_2F were dissolved in 1 mL Millipore Milli-Q water (MQ water) and 20 µl 8 M NaOH before being introduced into its respective culture. Expression for each mutant included a negative control which lacked addition of ncAA in culture. To check for protein expression in autoinduction media, 50 µl of pBAD-sfGFP (encode for expression of GFP) culture was added to 5 mL of autoinduction media and observations of green indicated protein expression in media.

Fifty mL of culture (WT and ncAA mutants) was pelleted at 3,750 rpm in a tabletop centrifuge for 10 minutes. Pelleted cells were stored in -80°C until further processing. Cell pellets were resuspended in 10 mL of Talon Equilibration buffer (50 mM sodium phosphate, 300 mM NaCl, pH 7.0) and passed through microfluidizer to collect the cell lysate. Cell lysate was centrifuged at 15,000 rpm for 20 minutes at 4°C. Talon Metal Affinity Resin was washed in 300 µl bed volume was added to each lysate supernatant. Mixture was shaken at 4°C for 20 minutes on platform shaker. Mixture was pelleted at 2,500 rpm for 5 minutes and resuspended in 5 mL of Talon Equilibration buffer. Resuspension was transferred to a sample-binding gravity-flow column. Purified proteins were eluted with 1.5 mL of Talon Elution buffer (50 mM sodium phosphate, 300 mM NaCl, 250 mM imidazole). The resin samples were added to the prepacked PD-10 desalting columns (GE Health Care). To desalt the resin bound protein, PD-10 desalting columns was washed with 2 mL Talon Equilibration buffer four times. Columns were then filled with 2.5 mL of 0.04 M phosphate buffer to elute protein bound to resin. The run-through was collected in 500 µl aliquots and stored at 4°C.

Qualification of protein expression by SDS-Page Gel. Glass plates (0.75 mm) were used to make a 15% SDS-Page gel according to manufacturer's instructions (Bio-Rad SDS-PAGE Mini Protein II system discontinuous Laemmli gels). The 15% separating gel was made with the following: MQ water, 30% polyacrylamide, 1.5 M, pH 8.8 Tris-HCl, 10% Ammonium persulfate, 10% SDS, and TEMED. The 5% stacking gel was made with the following: MQ water, 30% polyacrylamide, 0.5 M pH 6.8 Tris-HCl, 10% Ammonium persulfate, 10% SDS, and TEMED. 10x running buffer (250 mM Tris, 1.92 M Glycine, 1% SDS, pH 8.3) and 2x SDS loading dye (125 mM Tris-HCl, 4% SDS, 20% glycerol, 0.02% bromophenol blue, 5% **β**-mercaptoethanol, pH 6.8) was prepared. Samples (10 µl) were prepared by adding 20 µl of SDS-Sample buffer, heated for 5 minutes at 95°C, and spun down on centrifuge. Bio-Rad Precision Plus Dual Color molecular weight marker (4 µl) and 20 µl sample was used. Gel ran in 1x running buffer at 100 V. Gel was visualized by Coomassie Brilliant Blue stain.

Quantification of protein expression by Bradford assay. Concentration of protein samples was determined by Bradford Assay according to manufacturer's incrustations (Bio-Rad Quick Start Bradford Assay). Absorption of bovine serum albumin (BSA) as a standard was measured at 595 nm via spectrophotometry with 1 mL cuvettes. Concentrations of BSA used were 0.125, 0.25, 0.5, 0.75, 1, 1.5, and 2 mg/mL. Plotted values of known protein concentration versus absorption allow for linear regression calculation. This linear function allows for estimate of protein concentration of samples.

Qualitative and quantitative measurement of enzymatic function. For qualitative assay, 1 M p-nitrophenyl acetate (PNPA) was prepared in acetonitrile. Purified enzyme (0.00024 mg/mL) was added with 10 mM PNPA in the form of droplets for a total volume of 50 µl (*16*). For quantitative assay, velocity of HCA II was determined by measuring absorbance at 512 nm over time through the hydrolysis of PNPA. This was repeated in triplicate for different concentrations of substrate PNPA (*16*). We plotted the relative velocity over different concentrations to determine enzymatic rate, kcat and km, through a Michaelis Menten model (*16*). Quantitative assay was carried out at pH 7.4 and pH 6.4.

Protein Stability through Differential scanning fluorimetry. DSF was used to assess protein conformational stability in terms of melting temperature (T_M). Samples of purified WT HCA II and ncAA mutants at a concentration on 0.02 mg/mL were incubated on ice with 2x Sypro-Orange dye (S5692; Sigma-Aldrich) and 0.04 M phosphate buffer (pH from 5.4 to 9.4) (*17,18*). Final volume of each sample was 50 µl and ran in triplicate. Melting curve assays were conducted in a real-time PCR Machine (CX1000, Bio-Rad) with temperature ramping from 28°C to 99°C, increasing at a rate of 0.5°C every 5 seconds. Runs containing only buffer were also conducted in the same manner to be used to subtract background signal during data processing. The melting temperature (T_M) was defined as the maximum negative value of the first derivative data collection (dRFU/dT; change in fluorescence change in temperature) of the signal which is produced in terms of relative fluorescent units (RFU).

RESULTS AND DISCUSSION

Incorporation of ncAAs verified via SDS-PAGE gel. SDS-page gel was used to verify expression of HCA II and integration of ncAAs (Supplemental Figure 1). Without ncAAs in the media, TAG (at site 93) encoded for genome expansion machinery will be translated as a stop codon resulting in a truncated protein about 10 kDa in size. This negative control allowed us to easily visualize if ncAAs were incorporated into HCA II at its target site. When ncAAs are present in the media, the full-length HCA II is expressed at 29 kDa. This allows us to verify crude total protein on SDS-PAGE gel for intercession of desired ncAAs. Crude extract at time point zero shows little expression of HCA II; whereas, expression of crude extract of wildtype after 48 hours of induction shows a prominent band at 29 kDa. Expression of HCA II at 29 kDa is quickly apparent and can be confirmed by the lack of a 29 kDa band in the negative controls (Supplemental Figure 1). If the truncated protein was expressed, it may run off the gel due to its small size.

Purification and quantification of expressed WT HCA II and mutants. For future catalytic and stability assays, HCA II was purified from cell culture by microfluidizer and bound to a column (*14*). HCA II that is expressed includes an N-terminal 6x-His Tag which allows for metal binding to the column by Talon Bed affinity resin. Total cell lysate, collected wash, and purified protein was prepared and run on SDS-PAGE gel (Supplemental Figure 2). In both the total cell lysate and purified HCA II protein, a band at 29 kDa is present and in very high purity of at least 95% (Supplemental Figure 2). Since both ncAA mutants are the same size as our wild-type HCA II, we can conclude that the genetic code expansion system is functional and that the desired ncAAs are incorporated into the protein.

To assess concentration of purified protein, which is necessary for catalytic function studies, a Bradford assay was carried out (Supplemental Figure 3). With a known one-to-one correlation of protein absorption at 595 nm and protein concentration, a Bradford Assay was used with samples containing known protein concentrations of BSA to develop a linear regression used to predict protein concentration. A 95% confidence interval was calculated to show high confidence in values predicted. Values for concentration and yield of HCA II expressed can be found in Table 1. While expression of HCA II is not linked to ncAA incorporation, we do see an interestingly large increase in expression when adding pBrF into the protein.

Table 1: Total protein concentration and yield

Mutant	Concentration (mg/mL)	Yield (mg/L)
WT HCA II	0.2 ± 0.1	10 ± 1
pBrF Mutant	0.8 ± 0.1	40 ± 1
pNO_2F Mutant	0.1 ± 0.1	5 ± 1

Enzymatic activity in WT HCA II and ncAA mutants. To access how ncAA mutants affect catalytic activity relative to wildtype, hydrolysis of PNPA, pH 7.4 was used due to the change in color upon breakdown (clear to bright yellow). This would allow us to measure absorption at 512 nm as it increases upon breakdown of PNPA. While carbon dioxide is the natural substrate in the human body, its conversion to bicarbonate is a reversible reaction making it difficult to study enzymatic activity (*19*). Purified WT HCA II and ncAA mutants, pBrF and pNO_2F, show enzymatic functionality with the breakdown of PNPA compared to buffer alone (Supplemental Figure 4A).

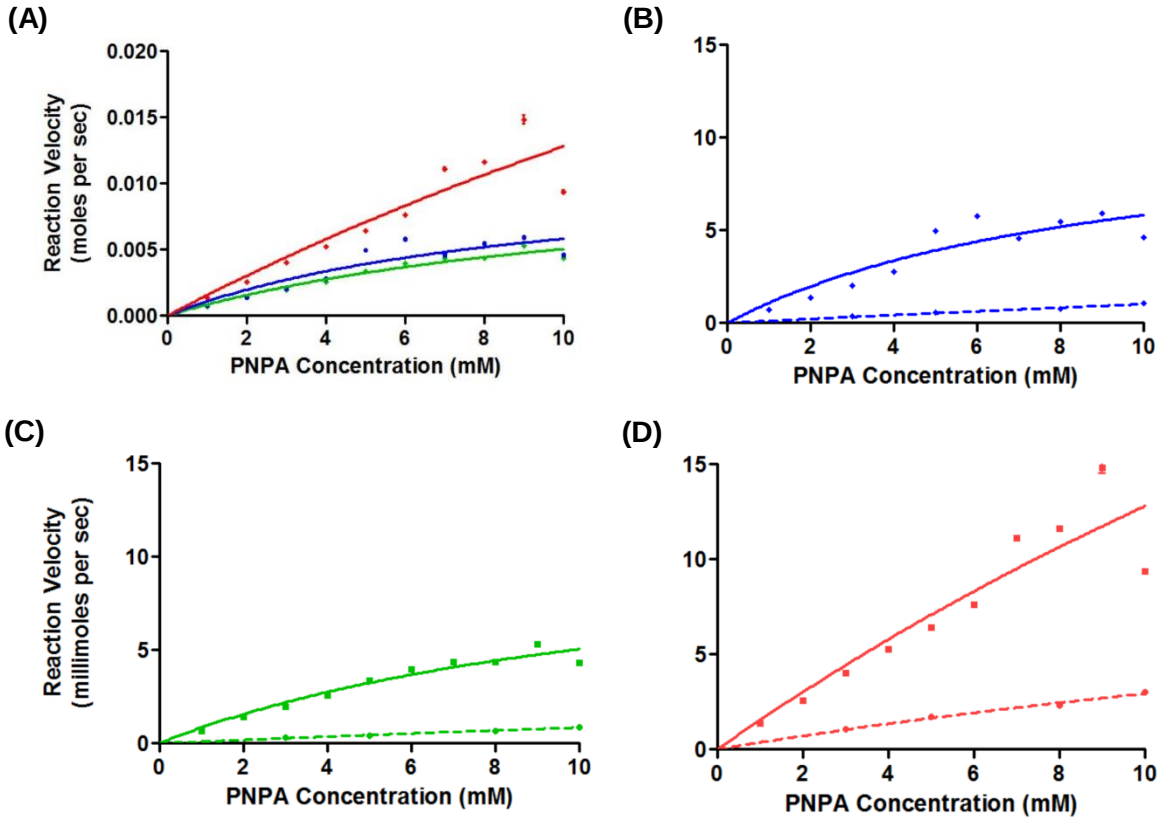

Figure 2: ncAA mutant pNO2F significantly improves catalytic function under neutral and acidic conditions. (A) WT HCA II is blue line, ncAA mutant pBrF is green line, and ncAA mutant pNO2F is red line. **(B)** WT HCA II in pH 7.4 is solid line and in pH 6.4 is dashed line. **(C)** pBrF mutant in pH 7.4 is solid line and in pH 6.4 is dashed line. **(D)** pNO_2F mutant in pH 7.4 is solid line and in pH 6.4 is dashed line.

To quickly access how change in substrate concentration affects enzymatic activity, differing concentrations of PNPA were hydrolyzed with equal amounts of protein (Supplemental Figure 4B). There is a clear correlation with increasing substrate concentration and increased enzymatic activity by the increase in color.

To determine enzymatic velocity, absorbance was measured over different concentrations of PNPA. The slope of the curve represents initial velocity. For each protein, 10 concentrations were assessed with a minimum of three replicates. What we found was particularly striking; under optimal pH conditions, the pBrF mutant shows a slight reduction in enzymatic activity and the pNO_2F mutant shows a significant increase in enzymatic activity (kcat and Vmax) compared to WT HCA II (Figure 2A, Table 2). For both ncAA mutants, there is an equal increase in the substrate binding constant, Km (Table 2). Error bars represent standard error of the mean (SEM). It is important to note that the enzymatic activity of the pNO_2F mutant is skewed higher due to three concentrations (PNPA 7, 8, and 9 mM) reaction velocity measurements being higher than our maximum concentration tested at 10 mM PNPA. This can be seen through the large error, which initially appear to negate these findings (Table 2). However, upon removal of these values and refitting of the curve, our error drops dramatically (Table 2). While the catalytic activity of the pNO_2F mutant is less of a substantial increase, it's more realistic. We are unclear on the cause of these skewed values, but we expect that upon further catalytic studies of these and nearby PNPA concentrations, this phenomenon would decrease within range of our other velocity values. Regardless, based on the kcat of the pNO_2F mutant,

Table 2: Kinetic values found in WT HCA II and ncAA mutants pBrF and pNO_2F.

	WT HCA II		pBrF Mutant		pNO_2F Mutant		
	pH 6.4	pH 7.4	pH 6.4	pH 7.4	pH 6.4	pH 7.4	pH 7.4[2]
Vmax (mmol/s)	0.6 ± 0.6	0.6 ± 0.1	0.5 ± 0.3	0.6 ± 0.1	0.8 ± 0.2	3.6 ± 3.0	1.2 ± 0.1
km (mM)	105 ± 103	9.6 ± 3.9	89 ± 62	12.6 ± 2.9	37 ± 10	42 ± 42	12.9 ± 1.7
kcat (s^{-1})	1.0 (± 0.9) x 10^7	9.9 (± 2.4) x 10^6	7.3 (± 4.7) x 10^6	1.0 (± 0.2) x 10^7	1.2 (± 0.3) x 10^7	5.8 (± 0.6) x 10^7	1.9 (± 0.2) x 10^7
Kcat/km (M^{-1} s^{-1})	9.5 x 10^1	1.0 x 10^3	8.2 x 10^2	7.9 x 10^2	3.2 x 10^2	1.4 x 10^3	1.5 x 10^3

we can conclude that the substrate binding pocket, mediated by the movement of the zinc atom, can hydrolyze PNPA faster. When compared to literature, we see identical relative hydrolysis of PNPA in WT HCA II (kcat/km ~ 1.0 x 10^3 $M^{-1}s^{-1}$) (*19*). For the pBrF mutant, we see a reasonable drop in hydrolysis (kcat/km ~ 7.9 x 10^2 $M^{-1}s^{-1}$) and the pNO_2F mutant, there was a reasonable increase (kcat/km ~ 1.5 x 10^3 $M^{-1}s^{-1}$) compared to literature values (*19*).

Since tumors which overexpress HCA II also have an acidic environment, catalytic activity was also measured at pH 6.4, one log less than initial catalytic activity measurements at pH 7.4. Again, enzymatic activity (kcat and Vmax) decreases for the pBrF mutant and increases for pNO_2F mutant compared to WT HCA II (Figure 2B-D, Table 2). However, substrate binding (km) for both ncAA mutants decreases compared to WT HCA II (Figure 2D, Table 2). This would suggest that under acidic conditions, PNPA binds more efficiently regardless of hydrolysis speed compared to WT. However, due to error and the limited number of concentrations used for fitting, we are unclear if these findings are due to a technical artifact.

Thermal Stability of WT HCA II and ncAA mutants. New mutations in catabolic residues often lead to a decrease in stability (*20*). In this study, new mutations were mediated by the introduction of selectively placed ncAA residues adjacent to residues in the active site. Differential scanning fluorimetry (DSF) was used as a quick, cheap, and high throughput method to assess the conformational stability of WT HCA II and ncAA mutants. A low concentration of 0.02 mg/mL of protein was tested with Sypro dye, which binds only to the hydrophobic regions of the protein that become exposed upon denaturation through heat (*21*,*22*). WT HCA II and ncAA mutants were tested for their thermostability, which was assessed under both optical pH conditions of 7.4 and under acidic conditions at pH 6.4 (Supplemental Figure 5A-B). Interestingly, the pNO_2F mutant is not only increased in catalytic efficiency but it is also more thermostable in optimal conditions (Figure 3, Supplemental Figure 5A). If the pH is lowered to 6.4, WT HCA II is relatively stable in comparison but pNO_2F mutant still shows high stability (Figure 3, Supplemental Figure 5B).

Previous literature has found a tradeoff between catalytic efficiency and protein stability; in general, optimized catalysts such as HCA II are less stable as a result (*23*). To test this trade off, we would expect our faster pNO_2F mutant to be less stable as a result when compared to WT. In addition, previous literature has found that HCA II increases in catalytic activity as pH increases (*2*). We would therefore expect that our WT mutant would decrease in stability as pH increased respectively. Upon expansion of a wide range of pH conditions ranging from pH of 5.4 to 9.4, we found that as expected, decreasing pH does lower catalytic activity and increase overall protein stability and with

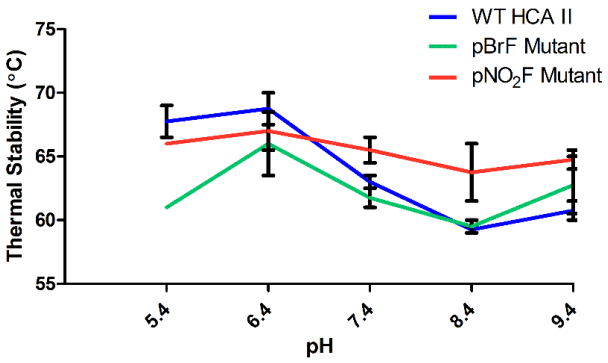

Figure 3: pNO2F is more thermostable than WT HCA II. Calculation of Tm of the protein based on the Boltzmann equation. Error bars represent SEM.

[2] Without using reaction velocities from 7, 8, and 9 mM PNPA.

increasing pH, protein stability decreases (Figure3, Table 2, Table 3). In addition, the pNO_2F mutant is overall more thermostable in harsh pH environments compared to thermostable WT HCA II despite its increased catalytic activity (Figure 3, Table 3). All the following thermostability data can be found in Table 3. Error bars represent standard error of the mean (SEM).

Table 3: Thermal Stability of WT HCA II and ncAA mutants[3]

	WT	pBrF Mutant	pNO_2F Mutant
pH 5.4	68 ± 1.3	61[§]	66[§]
pH 6.4	69 ± 1.3	66 ± 2.5	67 ± 1.5
pH 7.4	63 ± 0.5	62 ± 0.8	66 ± 1.0
pH 8.4	59 ± 0.3	59 ± 0.5	64 ± 2.3
pH 9.4	61 ± 0.8	63 ± 2.3	65 ± 0.8

CONCLUSION

This study's goal was to attempt to modulate cancer environments through the modification of residues adjacent to the active site with genetic code expansion. We hypothesized that by substituting Phe 93 with an electron withdrawing ncAA, we could probe the active site by shitting adjacent residues involved in maintaining a tetrahedral conformation with a zinc ion necessary for the hydrolysis reaction.

Previous studies using site-directed mutagenesis have shown that Phe 93 has little impact on the catalytic activity of HCA II (*8*). Our findings, however, contradict this; upon substitution of Phe 93 with pBrF using genetic code expansion, we see a slight decrease in catalytic activity and little change in stability compared to WT HCA II. Even more striking, the pNO_2F mutant has an increase in catalytic activity (kcat and Vmax) for pH conditions ranging from 6.4 to 7.4 and an increase in thermostability in pH conditions ranging from 7.4 to 9.4 when compared to WT HCA II. This significant increase shows that Phe 93 plays an important role in potentially stabilizing His 94, one of the three His residues involved in coordinating the zinc ion necessary for catalytic activity. We hypothesize its role is similar to other adjacent hydrophobic residues such as how Phe 95 helps stabilize His 96. Previous literature has suggested that the size of the amino acid at position 93 may increase the affinity to bind zinc and decrease the entropy loss associated with this process (*8*). In addition, previous work has suggested how weak C-H$\cdots\pi$ interactions between residues plays an important role in protein stability as seen in residues such as Phe 95 and Trp 97 (*24*). Both can potentially explain the phenomena we observe in the pNO_2F mutant; however, further studies must be carried out to determine the mechanism of this observed change.

While this work has some interesting findings, we would first want to carry out additional replicates for our kinetic assays under optimal and acidic conditions and collect additional replicants of the thermal stability of our proteins. In the future, we want to expand our studies using HCA II natural substrate, CO_2, and repeat all our catalytic studies. In addition, we would like to carry out ITC to better understand their binding characteristics between different mutants and substrates. In addition, we can determine thermodynamic parameters of interactions in solution. Allow us to study the binding of substrate molecules Finally, we would like to do x-ray crystallography to determine the structure for the ncAA mutants. This information will allow us to look at the positional change of residues involved the tetrahedral conformation of the zinc ion. We would also look at the respective movement of the beta-strand wall which is said to be anchored by the residue of interest, Phe 93. Further studies of this residue may lead to potential cancer treatments based on the pBrF mutant and industrial applications based on the pNO_2F mutant.

ACKNOWLEDGEMENTS

We would like to thank Dr. Ryan Mehl and Adian Estelle for insightful discussions on this work. We thank Dr. Kari van Zee for providing us Sypro Orange Dye. We also thank Dr. Jeff H. Chang for providing instrumentation for DSF.

REFERENCES

1. West, D., Kim, C., Tu, A., Robbins, A. H., Gruner, S. M., Silverman, D. N., and McKenna, R. (2012) Structural and kinetic effects on changes in the CO_2 Binding Pocket of Human Carbonic Anhydrase II. *Biochemistry* 51, 9156-9163.
2. Fisher, S. Z., Tu, C., Bhatt, D., Govindasamy, L., Agbandje-MKenna, M., McKenna, R., and Silverman, D. N. (2006) Speeding Up Proton Transfer in a Fast Enzyme: Kinetic and Crystallographic Studies on the Effect of Hydrophobic Amino Acid Substitutions in the Active Site

[3] Measured by melting point in terms of °C.

[§] Only represents one biological replicate.

of Human Carbonic Anhydrase II. *Biochemistry* 46, 3803-3813.

3. Wambo, T. O., Chen, L. Y., McHardy, S. F., and Tsin, A. T. (2016) Molecular dynamics of human carbonic anhydrase II in complex with Zn^{2+} and acetazolamide on the basis of all-atom force field simulations, *Biophysical Chemistry* 214-215, 54-60. doi: 10.1016/j.bpc.2016.05.006
4. Song, H., Wilson, D. L., Lewis, E. A., and Emerson, J. P. (2012) Revisiting zinc coordination in human carbonic anhydrase II. *Inord Chem* 51(20), 11098-11105.
5. Hurst, T. K., Wang D., Thompson R. B., and Fierke C. A. (2010) Carbonic anhydrase II-based metal ion sensing: Advances and new perspectives. *Biochimica et Biophysica Acta* 1804, 393-403.
6. Avvaru B. S., Busby S. A., Chalmers M. J., Griffin P. R., Venkatakrishnan B., Agbandje-McKenna M., Silverman D.N., and McKenna R. (2009) Apo-Human Carbonic Anhydrase II Revisited: Implications of the Loss of a Metal in Protein Structure, Stability, and Solvent Network. *Biochemistry* 48, 7365-7372.
7. Cox, J. D., Hunt, J. A., Compher, K. M., Fierke, C. A., and Christianson, D. W. (2000) Structural influences of hydrophobic core residues on metal binding and specificity in carbonic anhydrase II. *Biochemistry* 39, 13687-13694.
8. Hunt, J. A. and Fierke, C. A. (1997) Selection of Carbonic Anhydrase Variants Display on Phage. *Journal of Biochemical Chemistry* 272(33), 20364-20372.
9. Kean, K.M., Porter, J.J., Mehl, R.A., and Karplus, P.A. (2017) Structural insights into a thermostable variant of human carbonic anhydrase II. *Protein Science*. DOI: 10.1002/pro.3347
10. Haapasalo J., Nordfors, K., Järvelä, S., Bragge, H., Rantala, I., Parkkila, A-K., Haapasalo, H., and Parkkila, S. (2007) Carbonic anhydrase II in the endothelim of glial tumors: a potential target for therapy, *Neuro-Oncology* 9(3), 308-313. doi: 10.1215/15228517-2007-001
11. Leppilampi, M., Koistinen, P., Savolainen, E-R., Hannuksela, J., Parkkila A-K., Niemela, O., Pastorekova, S., Pastorek, J., Waheed, A., Sly, W. S., Parkkila, S., and Rajaniemi, H. (2002) The expression of carbonic anhydrase II in hematological malignancies, *Clinical Cancer Research* 8(7), 2240-2245.
12. Kato, Y., Ozawa, S., Miyamoto, C., Maehata, Y., Suzuki, A., Maeda, T., and Baba, Y. (2013) Acidic extracellular microenvironment and cancer. *Cancer Cell International* 13(89), 1-8.
13. Jackson J. C., Duffy S. P., Hess K. R., and Mehl R. A. (2006) Improving Nature's Enzyme Active Sites with genetically Encoded Unnatural Amino Acids., *Journal of American Chemical Society* 128, 11124-11127.
14. BB494 Biochemistry Lab Manual (Winter 2018) 1-47.
15. Hammill J. T., Miyake-Stoner S., Hazen J.L., Jackson J.C., and Mehl R.A. (2007) Preparation of site-specifically labeled fluorinated proteins for 19F-NMR structural characterization. *Nature Protocols* 2(10), 2601-2607.
16. Anderson J., Byrne T., Woelfel J., Meany J. E., Spyridis G.T., and Pocker Y. (1994) The hydrolysis of *p*-nitrophenyl acetate: a versatile reaction to study enzyme kinetics., *Journal of Experimental Education* 71(8), 715-718.
17. Abbott, J.A., Livingston, N.M., Egri, S.B., Guth, E., and Francklyn, C.S. (2017) Characterization of aminoacyl-tRNA synthetase stability and substrate interaction by differential scanning fluorimetry. *Methods* 113, 64-71.
18. Mahon, B.P., Lomelino, C.L., Salguero, A.L., Driscoll, J.M., Pinard, M.A., and McKenna, R. (2015) Observed surface lysine acetylation of human carbonic anhydrase II expressed in *Escherichia coli*. *Protein Science* 24, 1800-1807.
19. Gould, S. M. and Tawfik, D. S. (2005) Directed Evolution of the Promiscuous Esterase Activity of Carbonic Anhydrase II. *Biochemistry* 44, 5444-5452.
20. Tokuriki N., Stricher F., Serrano L., and Tawfik D. S. (2008) How Protein Stability and New Functions Trade Off. *PLOS Computational Biology* 4(2): e1000002. https://doi.org/10.1371/journal.pcbi.1000002
21. Matulis D., Kranz J. K., Salemme F. R., and Todd M. J. (2005). Thermodynamic Stability of Carbonic Anhydrase: Measurements of Binding Affinity and Stoichiometry Using ThermoFluor., *Biochemistry* 44, 5258-5266.
22. Rosa N., Ristic M., Seabrook S. A., Lovell D., Lucent D., and Newman J. (2015). Meltdown: A Tool to help in the Interpretation of Thermal Melt Curves Acquired by Differential Scanning Fluorimetry., *Journal of Biomolecular Screening* 20(7), 898-905.
23. Roca, M., Liu, H., Messer, B., and Warshel, A. (2007) On the Relationship between Thermal Stability and Catalytic Power of Enzymes. *Biochemistry* 46(51), 15076-15088.
24. Boone, C.D., Gill, S., Tu, C., Silverman, D.N., and McKenna, R. (2013) Structural, catalytic and stabilizing consequences of aromatic cluster variants in human carbonic anhydrase II. *Archives of Biochemistry and Biophysics* 539(1), 31-37.

SUPPLEMENTAL MATERIAL

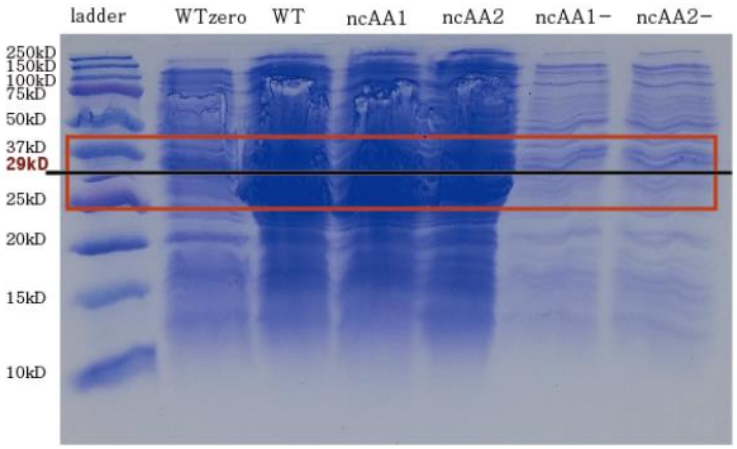

Supplemental Figure 1. Expression of Carbonic Anhydrase II from crude cultures. SDS-PAGE gel with crude cultures from left to right: WT_{zero} is from the original starter culture grown in non-induction media, WT is CA, ncAA1 is WT HCA II with the addition of pBrF, ncAA2 is WT HCA II with the addition pNO_2F, ncAA1- and ncAA2- is WT HCA II without respective ncAAs grown in autoinduction media.

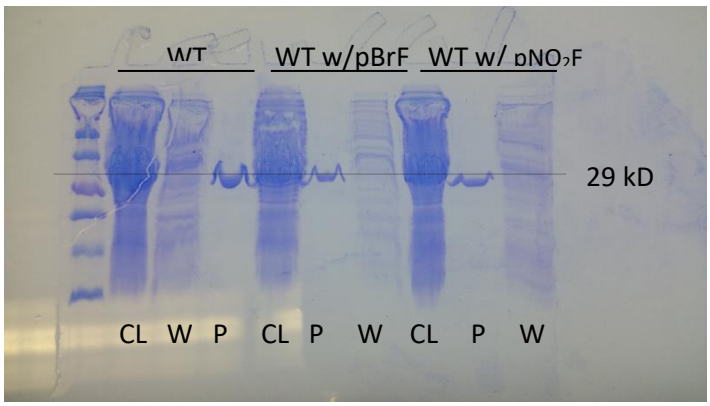

Supplemental Figure 2: Expression of Purified WT Carbonic Anhydrase II and ncAA mutants. SDS-PAGE gel with presence of purified WT HCA II at 29 kD. From left to right includes cell lysate (CL), elution (P), and washes (W) for WT, WT with pBrF and WT with pNO_2F respectively.

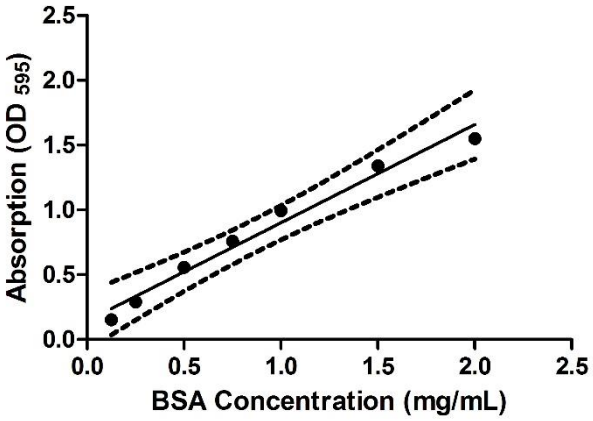

Supplemental Figure 3: Bradford Assay determines concentration of expressed HCA II. Linear regression of known protein concentrations with associated absorption allow for prediction of sample concertation. R^2 value indicates a one-to-one correlation with absorption and concentration. Dashed lines represent 95% Confidence interval.

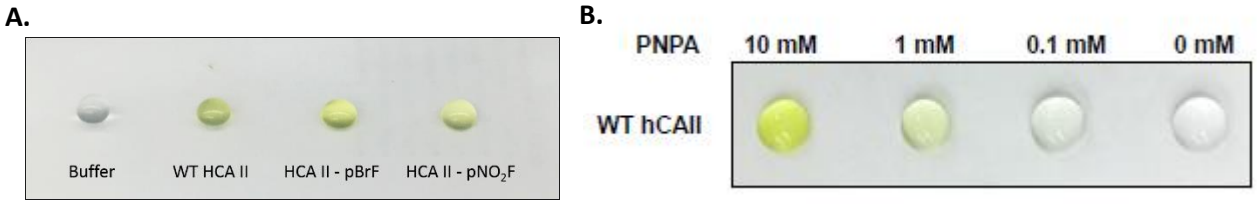

Supplemental Figure 4: WT HCAII and ncAA mutants display enzymatic functionality. (A) WT HCAII and mutants are catalytically active. Yellowing in color indicates hydrolysis of indicator compound PNPA. A negative control containing of water was used. **(B)** Rate of reaction decreases with decreasing substrate concentration. Yellowing in color indicates hydrolysis of indicator compound PNPA. A negative control containing of water was used. Rate of reaction of HCA II is altered based on concentration of substrate present.

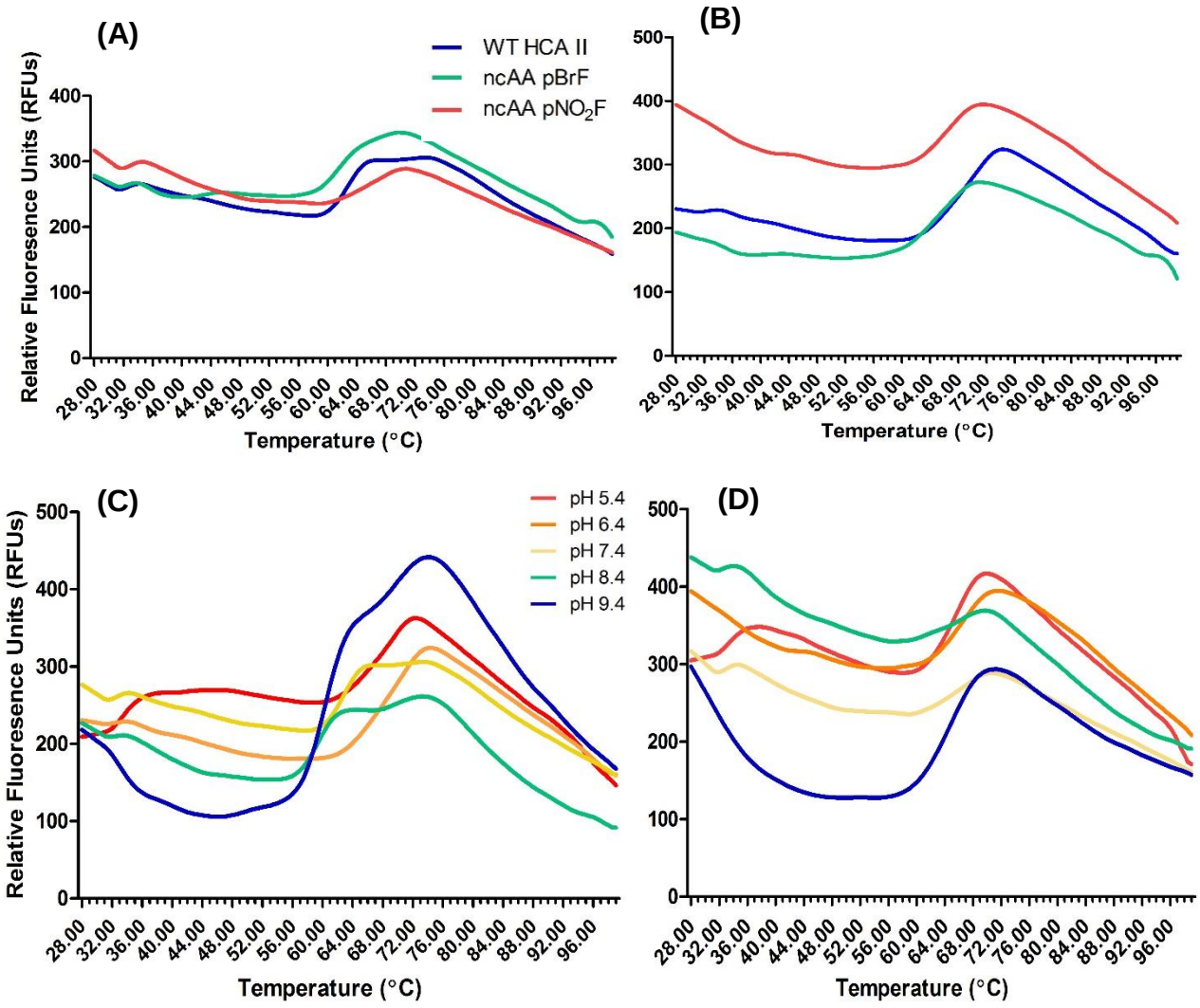

Supplemental Figure 5: pNO_2F Mutant is more thermostable than WT HCA II under optimal to basic conditions. (A) Thermostability of proteins of interest at pH 7.4. Tm is determined based on the Boltzmann equation. **(B)** Under acidic conditions (pH 6.4), stability of ncAA proteins is less than WT HCA II. **(C)** WT HCA II stability is highly affct by pH conditions. **(D)** pNO_2F Mutant is more thermostable under harsh pH conditions (pH 7.4 to 9.4).